J Mol Model (2013) 19:1339–1353
DOI 10.1007/s00894-012-1669-8

ORIGINAL PAPER

Electronic structure and decomposition reaction mechanism of cyclopropenone, phenylcylopropenone and their sulfur analogues: a theoretical study

Shabaan A. K. Elroby · Saadullah G. Aziz · Rifaat Hilal

Received: 18 September 2012 / Accepted: 29 October 2012 / Published online: 28 November 2012

Abstract The electronic structure, the origin of the extraordinary stability and the reaction mechanisms of the decomposition reaction of the three-membered ring cyclopropenone (IO), its phenyl derivative (IIO) and its sulfur analogues (IS and IIS) have been investigated at the B3LYP/6-311+G** level of theory. All critical points on the reaction surface, reactants, transition states and intermediates were determined. Reaction rate constants and half-lives have been computed. Natural bond orbital (NBO) analysis has been used to investigate the type and extent of interaction in the studied species. Results indicate that the decomposition reaction occurs via a stepwise mechanism, with the formation of a short-lived intermediate. The characters of the intermediates for the decomposition of IIO and IIS are different. In case of IIO decomposition, the intermediate structure is of prevailing zwitterionic character, whereas that for the decomposition of IIS is of prevailing carbene character. Solvent effects are computed, analyzed and discussed.

S. A. K. Elroby · S. G. Aziz · R. Hilal (✉)
Chemistry Department, Faculty of Science, King Abdulaziz University, Jeddah, Saudi Arabia
e-mail: rhilal@kau.edu.sa

S. A. K. Elroby
Chemistry Department, Faculty of Science, Beni-Suief University, Beni-Suief, Egypt

R. Hilal
Chemistry Department, Faculty of Science, Cairo University, Giza, Egypt

Keywords Density functional theory · Phenylcyclopropenone · Natural bond orbital · Zwitterion · Decomposition reaction

Introduction

Cyclopropenone was first synthesized in solution [1–3]. Cyclopropenone is a molecule of considerable theoretical interest, since it combines remarkable stability with extreme strain. Various physical studies [4] suggest that much of its stability is derived from the special conjugative stabilization of the two-π electron systems. In addition, cyclopropenone has a number of interesting chemical properties [5, 6] that suggest it could be a useful synthetic intermediate. Several theoretical and experimental studies on cyclopropenones and cyclopropenethione have been carried out to understand the electronic structure, spectroscopy and the stability of these compounds [7–19]. The photochemical and thermal decarbonylation of cyclopropenones to produce acetylenes and carbon monoxide [20–27] is displayed in Scheme 1.

In spite of the importance of this decomposition reaction, the literature does not seem to contain any systematic study of its mechanism. It is the aim of the present work to quantitatively explore the mechanism of the decomposition reaction of cyclopropenone, its phenyl derivative and its sulfur analogue. High level theoretical models within the framework of density functional theory (DFT) will be used to explore critical points on the decomposition reaction path. Bonding characteristics and conjugative interactions will be analyzed and discussed for transition states and stable intermediate species. Natural bond orbital (NBO) analysis will

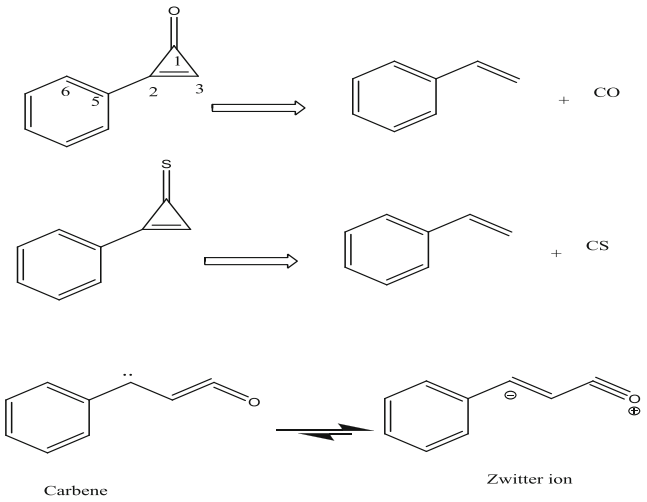

Scheme 1 Decarbonylation of cyclopropenones to produce acetylenes and CO

be used to give a deeper insight into the bonding characteristics of these species.

Computational methods

All calculations were performed using the Gaussian09W package [28]. The DFT/B3LYP method [29–31] was used throughout this work for exploring the mechanisms of the decomposition reactions of the studied compounds: cyclopropenone (IO), cyclopropenethione (IS), phenlcyclopropenone (IIO) and phenlcyclopropenthione (IIS). Critical points along the reaction paths were located and their geometries were fully optimized at the B3LYP/6-311+G** basis set [32] level of theory. B3LYP/6-311+G** frequency analysis calculations were performed to characterize the stationary points as the minima and transition states and to evaluate zero-point energies (ZPEs). In all calculations, transition state structures are characterized by one and only one imaginary frequency, while no imaginary frequencies were obtained for the minimum-energy species of reactants and intermediates. Intrinsic reaction coordinate (IRC) calculations [33, 34] were performed, starting at the transition states to check the reaction path of each reaction. Single point calculations were performed on the gas-phase optimized structures in order to include solvent effects. Those effects were computed within the framework of the self-consistent reaction field polarized continuum model (SCRF-PCM) [35–37] as implemented in Gaussian09W. Throughout the paper, we refer to the DFT wave function (i.e., Kohn-Sham orbitals) as molecular orbitals (MOs).

NBO calculations were performed at the B3LYP/6-311+G** level using NBO 3.1 as implemented in the Gaussian09W package in order to measure quantitatively the intramolecular delocalization in the studied systems. NBO theory [38, 39] has proved extremely useful in analyzing hyperconjugative [40] interactions through the second-order perturbation energy ($E^{(2)}$); which is estimated as:

$$E^{(2)} = \Delta E_{ij} = q_i \left(F_{ij}\right)^2 / \Delta\varepsilon$$

where q_i is the donor orbital occupancy, $\Delta\varepsilon$ is the difference between the energy of an acceptor orbital (j) and a donor orbital(i) and F_{ij} is the off-diagonal NBO Kohn-Sham matrix. The shape of highest occupied molecular orbital (HOMO) and lowest unoccupied molecular orbital (LUMO) orbitals were constructed using the Gauss View 5.0.8 visualization program [41].

Results and discussion

Cyclopropenone: origin of the extraordinary stability

Figure 1 presents the fully optimized geometric structure of IO charge densities on each atom and dipole moment vector computed at the B3LYP/6-311+G** level of theory. Some selected geometric parameters are given in Table 1. The

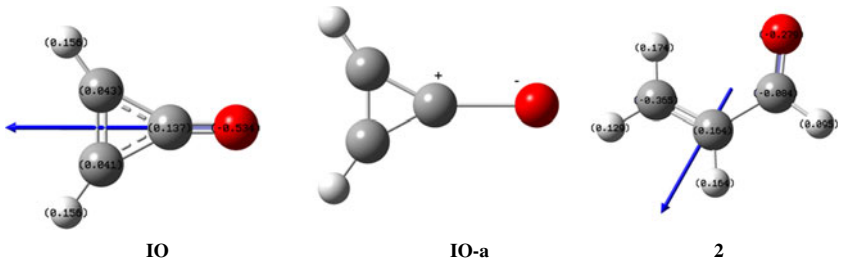

Fig. 1 Fully optimized geometric structure and Mulliken charge densities on each atom of cyclopropenone (IO), the ionic resonance structure (IO-a) and acroleine (2) contributing to the resonance hybrid structure of IO

Table 1 Comparison of the geometric parameters of cyclopropenone (IO) and that of cyclopropenthione (IS) calculated at the B3LYP/6-311+G** level of theory

Bond length (Å)	IS	IO	Angle (degrees)	IS	IO
R(1–2)	1.332	1.348	A(2-1-3)	61.9	62.1
R(1–3)	1.433	1.423	A(2-1-4)	144.3	147.7
R(1–4)	1.086	1.080	A(1-2-3)	62.00	62.1
R(2–3)	1.433	1.423	A(1-2-5)	144.6	147.7
R(2–5)	1.086	1.080	A(3-1-4)	153.8	150.3
R(3–6)	1.211	1.629	A(1-3-2)	56.1	55.8
			A(1-3-6)	151.9	152.1
			A(3-2-5)	153.5	150.3
			A(2-3-6)	152	152.1

correspondence between the theoretically computed and experimentally measured [12, 17, 18, 42] geometric parameters is excellent.

IO is a highly polar molecule with a dipole moment of 4.43 D (experimental value 4.39 D). This high polarity has been attributed to, and is a reflection of, the C=O bond polarity alone. This does not seem to be correct since, at the same level of theory, formaldehyde has a dipole moment almost half that of IO. The results of the present work reveal that the high dipole moment of IO may be attributed to the contribution of an ionic resonance structure (IO-a) to the resonance hybrid of IO. Let us examine the origin of the extraordinary stability of IO. The following discussion will go along three main lines. These are:

1. A discussion of charge density distributions in relation to the tightness of binding and C=O bond polarity.
2. An analysis and discussion of the frequency, amplitude and intensity of the C=O vibration, and
3. An NBO analysis of the interaction energy between the C=C and C=O bond orbitals.

In the analysis and discussion along these three lines comparison will be made with the isolated C=O case (formaldehyde) and the π-isoelectronic molecule acrolein

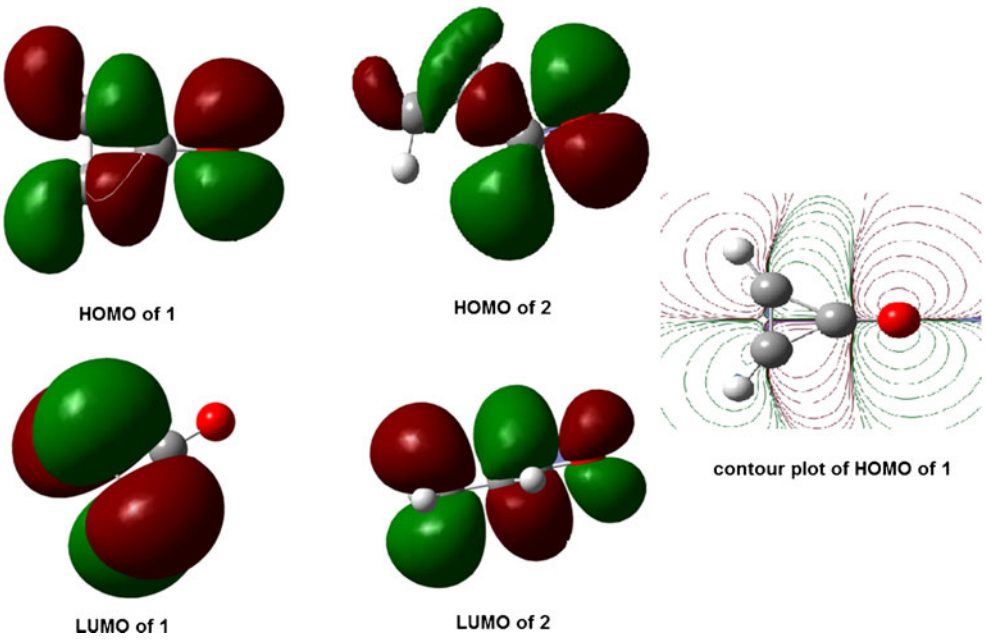

Fig. 2 Plots of the charge distribution of the frontier orbitals of IO and **2**

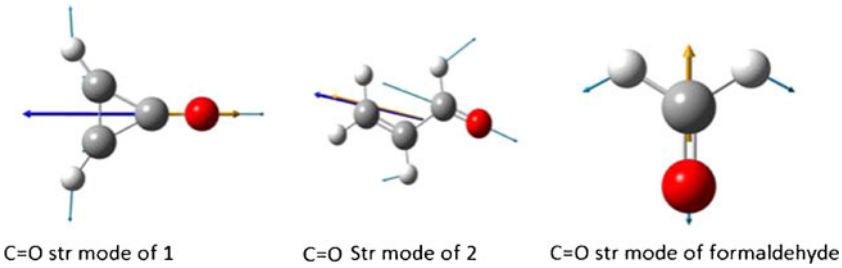

Fig. 3 C=O stretching modes for IO, **2** and formaldehyde. *Blue arrows* Direction of the dipole moment, *brown arrows* show direction of the dipole moment unit vector, *pale blue arrows* direction and amplitude of the displacement vectors

(**2**). Figure 2 presents the frontier MOs of IO and those for the π-isoelectronic acrolein. The molecular charge distribution in the MOs presented in this figure indicates clearly the tightness of binding in IO relative to that of acrolein. In the MOs presented, the charge distribution extents over the entire molecular framework. The contour plot of the HOMO of IO reveals that the p_z orbital at C1 plays a central role in this respect.

It is this p_z orbital that is engaged in and is responsible for the tight binding between the C=C and the C=O π-systems. In IO, the C=O bond shows a marked ionic character, with the O atom carrying about 0.6 e, which is almost double that on the O atom in acrolein or formaldehyde (0.3 e). This ionic character of the C=O bond facilitates the formation of the ionic resonance form IO-a and is responsible for the higher polarity of this compound. Figure 3 presents the C=O vibrational modes for IO, **2** and formaldehyde. The C=O vibration in formaldehyde is coupled strongly with the HCH angle bending (scissoring) vibration and appears with moderate intensity (118) at 1,650 cm^{-1}. In the case of **2**, the C=O vibrational mode seems to show weak coupling with the C=C vibrations and shows a shift to slightly higher frequencies to appear at 1,770 cm^{-1} with a greater amplitude and more than double the intensity (275) observed in the case of formaldehyde. The situation is completely different in the case of IO, where the C=O vibration mode couples strongly with the C=C bond vibrations and is shifted up field considerably to appear at 1,900 cm^{-1} with a very large amplitude and very strong intensity (800).

Decomposition reaction of cyclopropenone

The thermal decomposition of IO might proceed via a concerted mechanism in which the two C–C bonds undergo

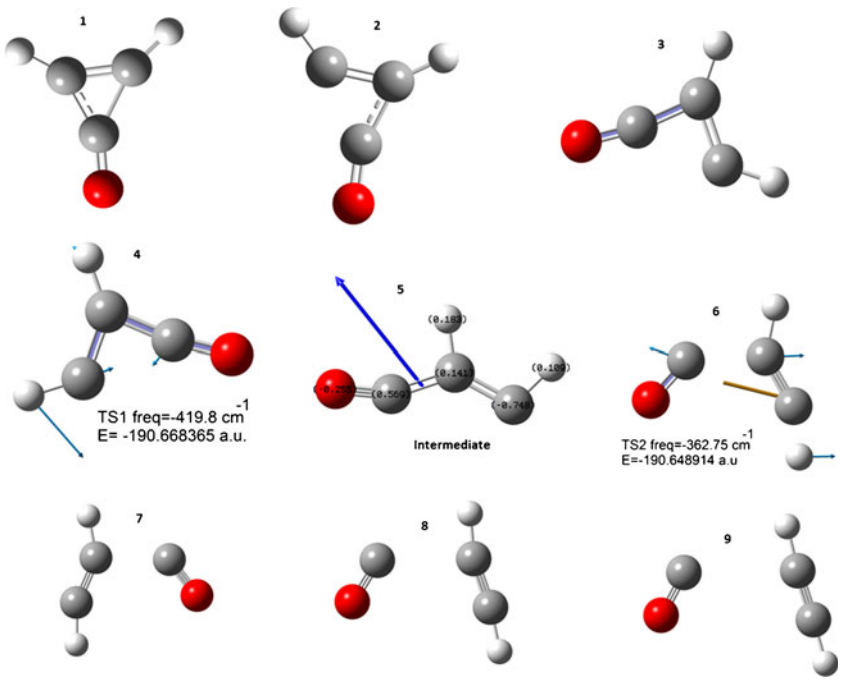

Fig. 4 Geometry changes along the decomposition reaction path of IO

cleavage simultaneously, or it may follow a two-step mechanism; i.e., a step-wise mechanism in which a ring rapture is a first step, which leads to an intermediate that will undergo a C–C cleavage to form the products. We have examined these two routes. The potential energy change for the concerted mechanism is very much steeper than that of the stepwise mechanism. The concerted pathway leads to a very high energy barrier of >100 kcal/mol^{-1} and, therefore, this route is not likely and will not be investigated further. A search along the stepwise mechanism for critical points was conducted on three levels. A scan on the C1–C3 bond stretching coordinate was carried out leading to a critical point identified as the transition structure along this route. Optimization and subsequent frequency calculations revealed that this is a saddle point on the reaction energy profile characterized by one, and only one, negative frequency. This transition state (TS1) is presented in Fig. 4. It should be noted that this transition state is only 31.7 kcal/mol^{-1} above IO and is characterized by a moderate imaginary frequency (419 cm^{-1}), indicating the low curvature of the potential energy profile. This vibrational mode is a coupling between the C1–C3 stretching and the C1–C3–C2 angle bending (scissoring) mode. The second step of the decomposition reaction did not start until C1–C3 is almost broken (1.88 Å) where the C2–C3 bond stretches until CO and acetylene are formed. Figure 4 presents the transition state along this route (TS2). This transition structure is much less polar than IO (μ=0.82 D) and the potential energy profile seems to be of much lower curvature, with a vibrational mode corresponding to the C2–C3 stretching going down smoothly to products. The different curvatures and corresponding reaction modes indicate clearly that the decomposition reaction takes place in two consecutive steps. Figure 4 presents the two transition states, the intermediate structure and some snapshots along the reaction path. The intermediate shows a considerable separation of charge and is highly polar, suggesting a zwitterionic character.

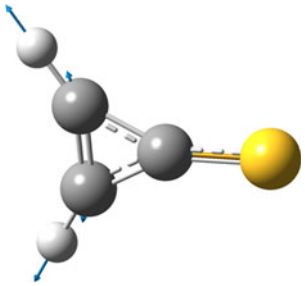

Fig. 6 The 1,429 cm^{-1} vibration C=S mode strongly coupled with ring vibration (indicated by *pale blue arrows*)

Cyclopropenthione

The fully optimized geometric structural parameters of cyclopropenthione (IS) are compared to the corresponding parameters of IO in Table 1. The charge distribution and dipole moment vector are presented in Fig. 5. Data in Table 1 reveal a very slight effect on the geometry of the three membered ring of replacement of oxygen by sulfur. IS shows separation of charge at the C=S bond, with the sulfur atom carrying almost 0.38 e. IS is slightly more polar (μ=4.762 D) than IO and show salmost the same charge density distribution for its frontier orbitals as IO (*cf.* Figs. 2, 5).

The C=S vibrational mode in IS shows a completely different trend to that discussed before for the C=O stretching modes in IO and **2** or formaldehyde. In IS, the vibrational spectrum shows two main bands at 1,429 and 1,650 cm^{-1}. The intensity of the former vibration band is three times as strong as that of the latter. Both vibrational modes involve C=S stretching, yet are strongly coupled and dominated by ring vibrations. Figure 6 presents the 1,429 cm^{-1} vibration indicating the ring vibrations.

The decomposition of IS is highly endothermic as compared to that of IO. The decomposition mechanism of IS is also a stepwise mechanism similar to that of IO. The transition state of the first step, TS-1 and that of the second step TS-2 and the intermediate zwitterions structure are all displayed in Fig. 7.

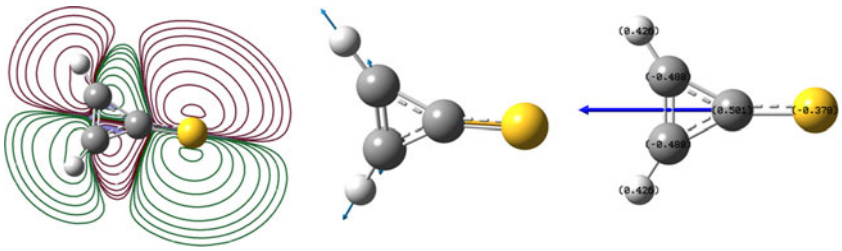

Fig. 5 Fully optimized geometry, Mulliken charge densities and dipole moment vector and contour plot of the HOMO of IS

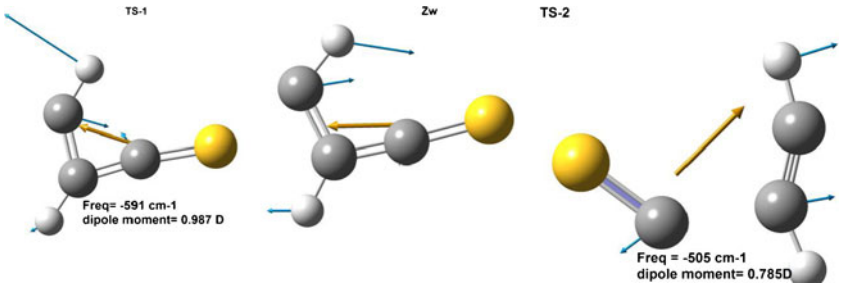

Fig. 7 Fully optimized structures for transition states and zwitterionic intermediate for the stepwise decomposition of IS

Phenylcyclpropenone and phenylcyclopropenthione

Let us now investigate the electronic structure and decomposition reactions of phenylcyclpropenone (IIO) and phenylcyclopropenthione (IIS). The equilibrium geometries of IIO and IIS are arrived at by full geometry optimization at the B3LYP/6-311+G** level of theory. These are presented in Fig. 8 together with the charge densities on each atom. All bond lengths in the IO ring in IIO are longer than the corresponding ones in IO. This may be attributed to the extended delocalization of the π system and, consequently, the decrease in the tightening of binding in the three-membered ring. IIS shows the opposite trend, however, where slight shortening of all bond lengths in the three-membered ring is observed. However, both molecules suffer considerable polarization of the charge density leading to greater dipole moments that amount to 5.46 and 6.13 D, for IIO and IIS, respectively.

The potential energy surfaces for the decomposition reactions were scanned to locate critical points. Transition states and intermediate structures were located and identified. The geometries of reactants, transition states and the intermediates for decomposition reaction of IIO and IIS in ground state were optimized unrestrainedly by means of the DFT/B3LYP. For the two reactions studied, we reported the gas-phase potential energy profiles calculated as relative energies (including ZPVE) of the species involved in the reaction pathways with respect to the ground-state reactant.

Figure 9 presents the geometries and charge density on each atom for all critical points located and identified on the potential energy surfaces for the two reactions studied. The presence of the phenyl ring does not alter the geometry of IO yet an increase in π-electron delocalization is observed. There is a general resemblance between the reaction routes taken by IIO, IIS and IO. First order transition states correspond in all cases to the rupture of the cyclopropenone ring

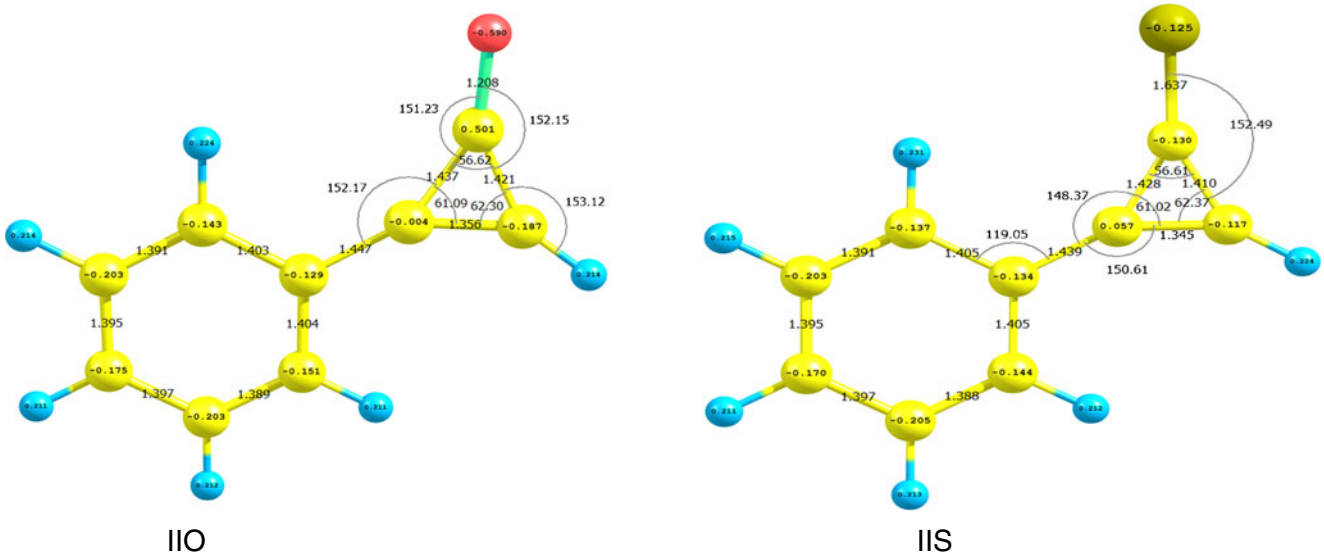

Fig. 8 Equilibrium geometries and charge densities on atoms for IIO and IIS

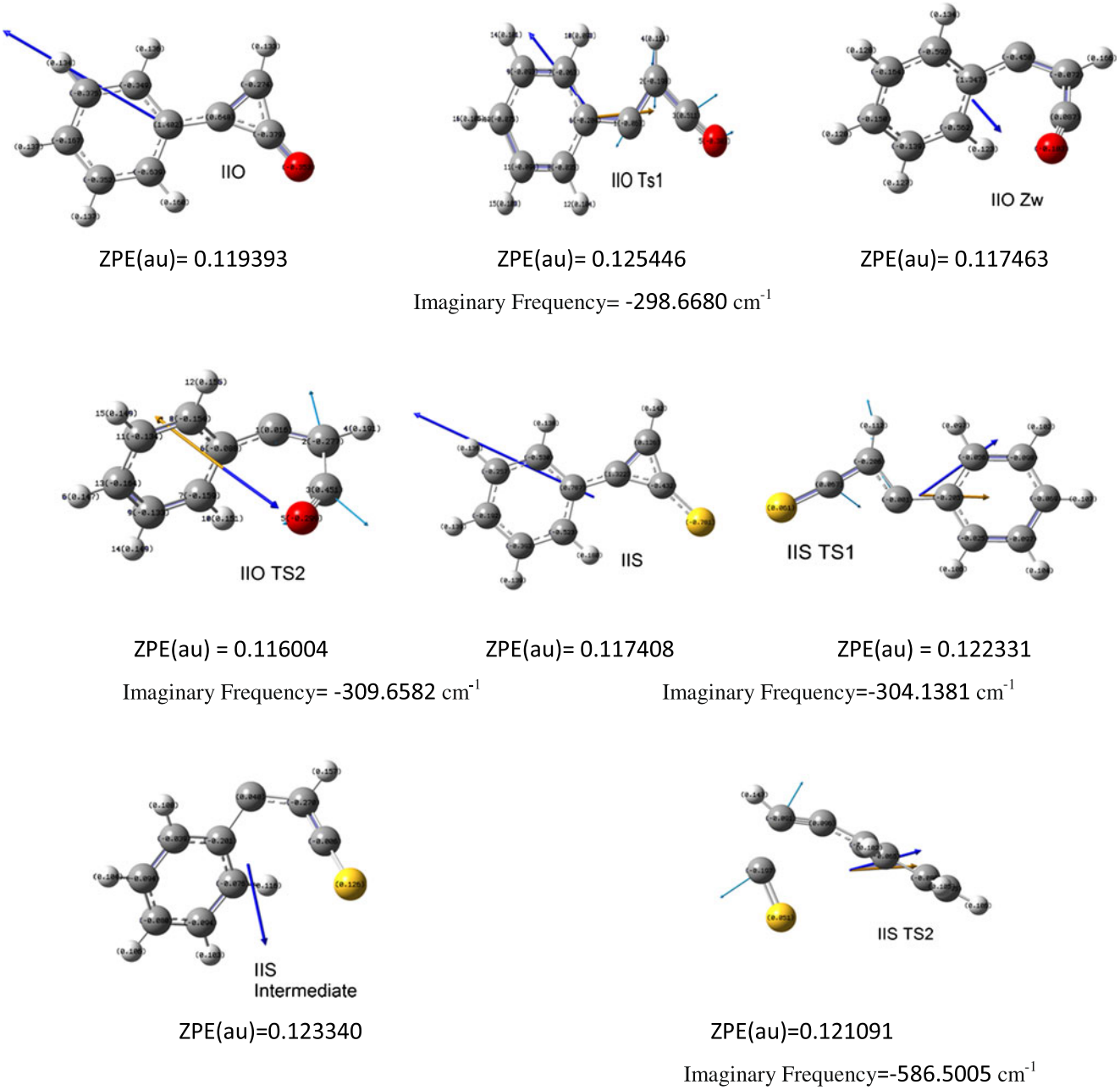

Fig. 9 Geometries, charge densities on atoms and dipole moment vectors of all critical points along the decomposition reaction path of IIO and IIS

followed by a second independent step involving the cleavage of the C–C bond forming CO and the corresponding acetylene.

Figure 10 shows a schematic diagram of the predicted reaction paths and activation energies for the decomposition of IIO and IIS. The first barrier height is calculated to be 26.33 and 37.73 kcal/mol^{-1} for IIO and IIS, respectively. In contrast to the case of the parent IO, the transition state for the first step in the decomposition of IIO and of IIS is higher in energy indicating that this step is the rate-limiting step of this reaction.

Figure 11 shows the IRC profile for TS1 of IIO. In the forward direction, the IRC calculations terminated with the formation of an intermediate structure, while the reverse

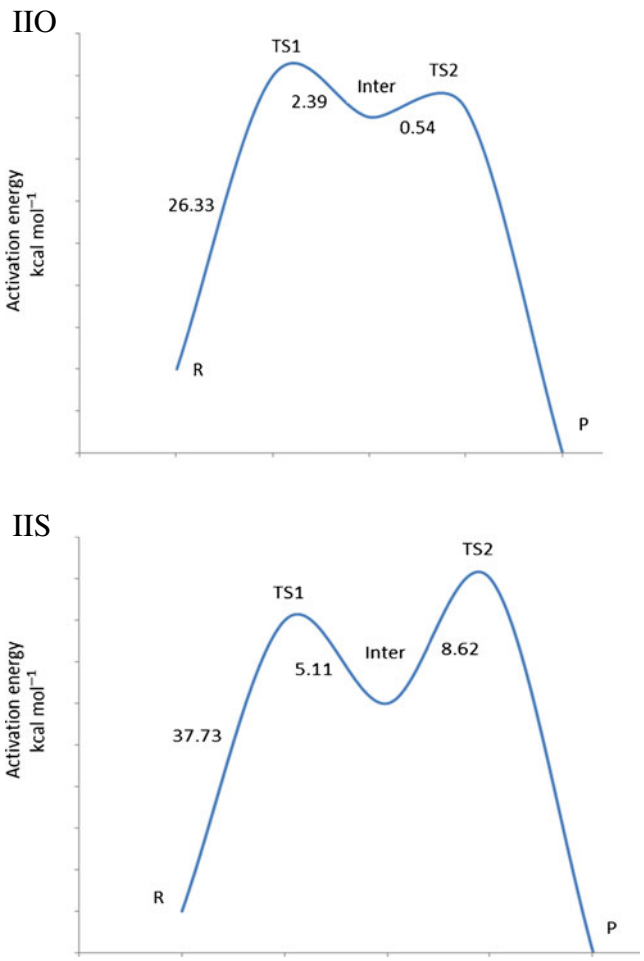

Fig. 10 Gas-phase potential energy profiles for the studied reactions. The relative energies (kcal/mol^{-1}) of the transition states and intermediates are calculated with respect to the ground-state reactant

direction leads directly to the parent phenylcyclopropenone. The present calculations, at B3LYP/6-311+G** level, confirmed that the TS1 first order saddle point does connect the reactant (IIO) and an intermediate and thus confirms the stepwise mechanism of this reaction. The IRC calculation for TS2 in the second step of the decomposition of IIO is depicted in Fig. 11. The present IRC calculations verified that the transition structure (TS2) connects the stable intermediate structure and the products. The second step in the decomposition reaction, i.e., the dissociation of the intermediate structure into CO and acetylenes, seems to be much faster due to the considerably lower barrier height, which amounts to 0.54 and 8.62 kcal/mol^{-1} for IIO and IIS, respectively. This would suggest that the intermediate structure for the decomposition reactions of IIO and IIS are of short duration; in agreement with pervious theoretical and experimental studies [12, 17, 18].

The nature of the stable intermediate structure

The PES for the decarbonylation of IIO and IIS, just as that for the parent molecule IO, shows that the loss of CO is a stepwise process. Synchronous cleavage of both C1–C3 and C2–C3 bonds is unlikely since the simultaneous increase in both carbon–carbon distances results in a steep rise in energy. The valley on the PES follows the elongation of one of the C–C bonds, while the other bond remains virtually unchanged. Only when the first single bond of the cyclopropenone ring is almost broken (at ca. 2.2 Å, which is little bit longer than that in case of IO), does cleavage of the second bond begin. The relaxed PES scan does not show the formation of the intermediate; however, geometry optimization in the two dimensional space governed by C1–C3 and C2–C3, in the region between TS1 and TS2, allowed us to locate the energy minimum. This structure has a C1–C3 distance of 2.23 Å, a C2–C3 of 1.36 Å. Frequency calculations confirmed that this structure corresponds to a real minimum since there are no imaginary frequencies. These results agree well with the previously reported DFT/CCSD study of the carbonylation of acetylene.

The phenyl substituents in IIO and IIS lie in the plane of the cyclopropenone ring, and both molecules are perfectly planar. Cleavage of the C1–C2 bond and the formation of the intermediate are accompanied by a substantial change in the molecular geometry and charge density distribution. Thus, the dipole moments are reduced substantially and smoothly on going through TS1, intermediate and TS2. There are also dramatic changes in geometry along this path. Thus, while IIO and IIS and the corresponding TS1 structures are perfectly coplanar, the intermediate structures loss this coplanarity where the phenyl ring at C2 moves from the *Z* arrangement with respect to the substituent at C2 in the starting geometry to a transoid position. The torsion angle amounts to 37° for both IIO and IIS.

In the case IIO, the first transition state (TS1) is characterized with only one imaginary frequency (−304 cm^{-1}), which corresponds to a coupling between the C1–C3 stretching and C2–C1–C3 angle bending modes. The imaginary vibrational modes associated with the only negative eigenvalue of the TS2 corresponds to the C2–C3 bond breaking. Some selected geometric parameters of TS1 and TS2 for the reactions studied together with charge distribution are shown in Table 2 and Fig. 12.

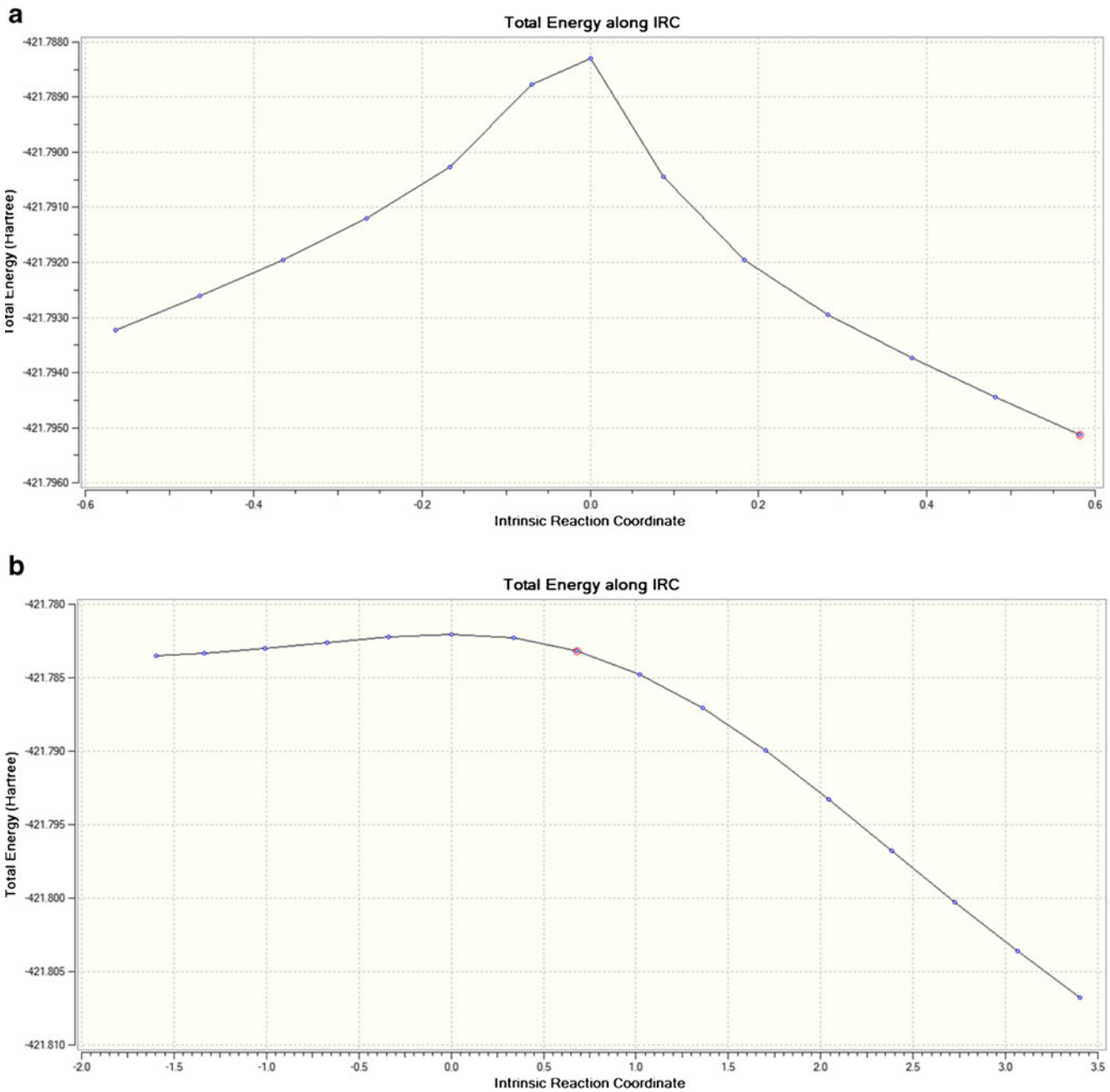

Fig. 11a,b Intrinsic reaction coordinate (IRC) for decomposition reaction for IIO computed by B3LYP/6-311+G**. **a** TS1 (**b**) TS2

The nature of the short-lived intermediate is somewhat controversial. Some previous studies suggested a carbine like-character, whereas others suggested a pure zwitterionic character for these short-lived intermediates. The geometry and charge distributions of the intermediate structures for the decomposition of IIO and IIS are shown in Fig. 12. Both intermediate structures are non-coplanar with an out of plan angle of 37°. It is well known that carbenes in general enjoy maximum conjugative interaction, forcing coplanarity of composite molecules. Furthermore, the IIO intermediate shows a considerable separation of charge in the ph-C bond region. Thus, C2 accumulates almost 0.5e, whereas the phenyl carbon atom carries a considerable positive charge of 1.347e. Furthermore, C–O and C2–C3 bond distances are about 1.151 and

Table 2 Optimized geometrical parameters of phenylcyclpropenone (IIO) and phenylcyclopropenthione (IIS) using B3LYP/6-311+G**

	R_{C1-C2}	R_{C1-C3}	R_{C2-C3}	R_{C2-C4}	R_{C1-O}	$<_{C4-C2-C1}$	$<_{C1-C3-C2}$	O	C2
IO									
Reactant	1.431	1.431	1.344		1.203		62.0	−0.574	−0.178
TS1	1.772	1.341	1.350		1.183		88.48	−0.504	−0.202
Inter	2.231	1.364	1.376		1.147		132.69	−0.395	−0.151
TS2		1.644	1.287		1.159		112.057	−0.433	−0.143
IIO									
Reactant	1.437	1.421	1.356	1.447	1.208	146.3	62.3	−0.590	−0.004
TS1	1.903	1.352	1.367	1.446	1.130	125.8	88.9	−0.429	−0.057
Inter	2.408	1.382	1.370	1.435	1.151	128.9	111.1	−0.391	0.076
TS2	2.359	1.578	1.289	1.412	1.156	142.94	111.0	−0.434	0.107
IIS									
Reactant	1.428	1.410	1.345	1.439	1.637	150.6	62.4	−0.125	0.057
TS1	2.007	1.334	1.387	1.463	1.546	123.4	95.0	0.218	0.013
Inter	2.430	1.323	1.438	1.460	1.536	118.0	122.3	0.269	0.046
TS2	2.325	1.701	1.238	1.411	1.553	159.4	103.5	0.183	0.116

1.370 Å respectively, which are very close to typical value of zwitterionic structures (C1–O=1.11 Å, C2–C3=1.35 Å) [17].

This charge separation together with the non-coplanarity of the intermediate structure suggests a prevailing zwitterionic character of this intermediate. On the other hand, the intermediate structure of IIS does not show any charge separation at all and hence one can assume a prevailing carbine like character for this intermediate. It should be noted that, in both cases, the intermediate is a resonance hybrid; however, the prevailing zwitterionic character dominates in the case of IIO and the carbine character dominates in case of IIS intermediate.

Kinetics and thermodynamic parameters

Let us examine the energetics of the decomposition reaction. Figures 10 and 13 present the potential energy profile for the decomposition of IIO and IO. The enthalpy changes of the decomposition reaction of IO (*cf.* Table 3), and IIO are −3.47 and −1.16 kcal/mol^{-1}, respectively, indicating the exothermic nature of the decomposition process. For the decomposition of IS and IIS, however, the reaction is endothermic (= 40.20 kcal/mol^{-1}). In the four reactions studied, the first step is the rate determining step, with activation energy barriers of 5.35, 32.64, 26.33 and 37.73 kcal/mol^{-1} for the decomposition reaction of IO, IS, IIO and IIS, respectively.

In the present work, the rate constant for the decomposition reactions studied were estimated from transition state theory (TST) formulation [43] using

$$k_{TST} = k_B T/h \exp\left(-\Delta G^{\#}/RT\right) \quad (1)$$

where k_B and h are Boltzmann's and Planck's constants, respectively, $\Delta G^{\#}$ is the change in the standard Gibbs free energy between the transition state and the reactant species (including the respective ZPEs). The results of the present calculations are presented as k_{TST} in Table 4. One can readily conclude that reactants, intermediates and products are all kinetically stable species at ambient temperature, although IIS is thermodynamically unstable with respect to the decomposition process.

The kinetic and thermodynamic parameters are shown in Table 4. Data in Table 4 reveal that the decomposition of IS is much slower. The rate determining step (first step) has an activation energy almost double that of IO, causing a considerable decrease in the reaction rate constant. The second step in the decomposition reaction resembles to a great extent that of IO in terms of reaction rate and duration.

Solvent effect

In the present work, solvent effects were computed using single point calculations on the gas-phase optimized geometries, using the SCRF-PCM approach. Three different solvents, namely water, DMSO and diethylether (DEE), were considered. The computed solvation energies and relative energies for the studied reactions are reported in Table 5. Solvent effects do not induce changes in the shape of the potential energy profile. All species in the decomposition reaction routes are more stable in solution. For example, in the case of IIO, reactant, TS1 and the stable intermediate are

Fig. 12 Most relevant geometrical parameters of the species involved in the decomposition reaction of the studied compounds (IIO, IIS). Bond distances are in angstroms and angles in degrees

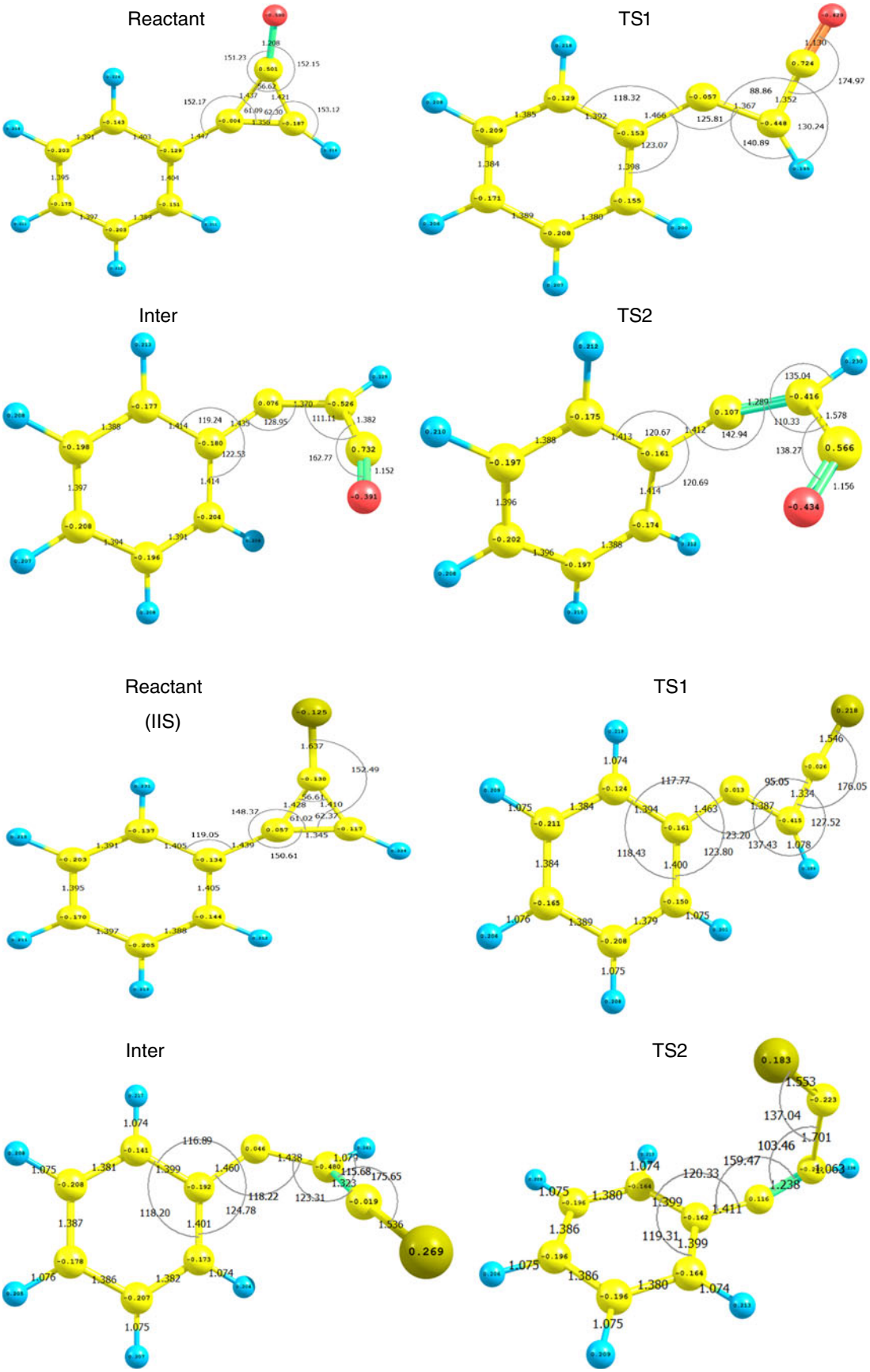
Reactant
TS1
Inter
TS2
Reactant
(IIS)
TS1
Inter
TS2

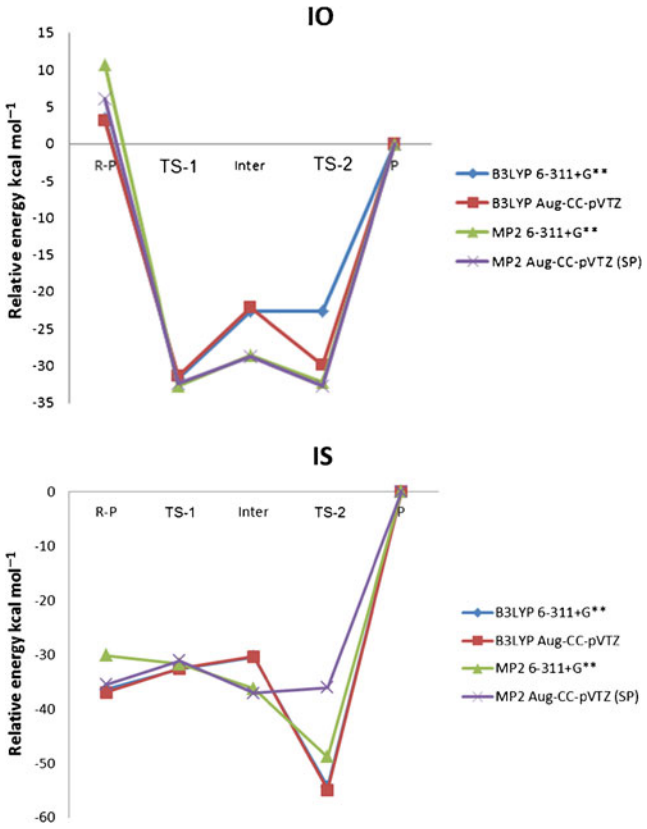

Fig. 13 The variation of the relative energies of all critical points on the decomposition reaction path of IO and IS with B3LYP and MP2 methods

stabilized by 11.62, 6.88 and 8.93 kcal/mol^{-1} in water as a solvent; computed values of relative energies indicate that, the initial barrier increases by about 0.94 kcal/mol^{-1} with respect to the gas-phase value. In the case IIS, the initial and third barriers increase by about 1.71 and 4.14 kcal/mol^{-1} with respect to the gas-phase value, respectively. In contrast, the second barrier decreases by around 2.37 kcal/mol^{-1}.

NBO analysis

Some selected NBO data are presented in Table 6. The natural population of the pz orbitals on the three carbon atoms and of the oxygen atom is shown in Table 6. The pz orbital of C3 is slightly higher in energy and less populated than that for C1 and C2. It should be noted that C3 is strongly involved in bonding via charge transfer interactions. Thus, it acts as electron donor via its 2 s and 2p orbitals, which lose charge to the π-system, and acts as electron acceptor via its Rydberg orbitals. Second order perturbation analysis of the Fock matrix indicates that the major interaction involves the $\pi_{C1\text{-}C2}$ bond orbital and the anti-bonding $\pi^*_{C3\text{-}O}$ bond orbital. This interaction amounts (E^2) to 86 kcal/mol^{-1} and is by far greater than all other interactions among the orbitals in IO. Worth noting also is the interaction of the oxygen lone pair orbital with the Rydberg orbitals of C3. This interaction amounts to, and is responsible for, the population of the virtual Rydberg orbitals of C3.

In conclusion, the extraordinary stability of IO may very well be attributed to

(1) The strong interaction between the C=C and the C=O bond orbitals and the consequent extension of the π-system
(2) The involvement of the C3 pz orbital in tightening of binding and imparting an "aromatic character" to 1, in addition to
(3) The contribution of the ionic resonance form IO-a to the resonance hybrid. This may also elaborate upon the suggestion of the "aromatic character" of IO.

The results of the NBO analysis (the stabilization energy $E^{(2)}$) for IIO and IIS compounds are given in Tables 7 and 8. Large $E^{(2)}$ values indicate a more intensive interaction between the electron donors and electron acceptors. The most important centers of interactions in the present study are LP of O and S/$\sigma^*_{C1\text{-}C3}$, $\sigma^*_{C1\text{-}C2}$, $_{\sigma C1\text{-}C2}/\pi^*_{C1\text{-}O}$, $\sigma_{C1\text{-}C3}/\pi^*_{C1\text{-}O}$ and $\sigma_{C2\text{-}C3}/\pi^*_{C5\text{-}C6}$. It is interesting to follow the trend of interaction between LP(O) and $\sigma_{C1\text{-}C3}$ along the decomposition reaction path. $E^{(2)}$ values decrease from reactant to TS2, whose contributions are 24.74, 8.34, 6.61, and 3.77 kcal/mol^{-1} for reactant, TS1, intermediate and TS2, respectively. As shown in Table 6, the hyperconjugative interactions between $\sigma_{C2\text{-}C3}$ and $\pi^*_{C5\text{-}C6}$ in the phenyl ring increase from reactant to TS2. These values support the proposed stepwise mechanism leading to phenylacetylene and carbon monoxide. The results of NBO analysis show that $E^{(2)}$ values corresponding to charge transfer from the phenyl ring to the C=C bond, in the three membered ring of IIS, are more pronounced than that in the case of IIO. In the case of the intermediate of IIO, the most important interaction energy is electron donation from $\sigma_{C3\text{-}C2}$ to the antibonding acceptor $\pi^*_{C5\text{–}C6}$ orbital with a stabilization energy of about 66.62 kcal/mol^{-1}. In contrast, the interaction between LPO and C1–C3 is of much lower value and amounts to 6.61 kcal/mol^{-1}. This is further evidence for the prevailing zwitterionic character of this intermediate structure.

Assessment and evaluation of the theoretical model

In order to assess and evaluate the computational approach used in the present study, computation at the MP2 levels of

Table 3 Comparison of the total energies (au) and relative energies (kcal/mol^{-1}) computed for the decomposition reactions of IO and IS at different levels of theory

		R	TS-1	Inter	TS-2	Product			
IO									
B3LYP	6-311+G**	−190.70030	−190.64975	−190.66407	−190.66415	−190.7056957			
	Aug-CC-pVTZ	−190.71846	−190.66827	−190.68299	−190.67070	−190.7234017			
MP2	6-311+G**	−190.1743198	−190.122244	−190.128763	−190.123048	−190.1914025			
	Aug-CC-pVTZ	−190.2967827	−190.2451854	−190.2509466	−190.2445641	−190.3064685			
IS									
B3LYP	6-311+G**	−513.6640781	−513.61205768	−513.615576	−513.577438276	−513.6060318			
	Aug-CC-pVTZ	−513.68429	−513.63241	−513.635913	−513.596787208	−513.625338			
MP2	6-311+G**	−512.7510306	−512.73364	−512.69323113	−512.673189907	−512.7029917			
	Aug-CC-pVTZ	−512.8822433	−512.8326694	−512.8231051	−512.8247355|	−512.8256417			
Relative energies									
Method	Basis set	R-TS				P-TS			
		R-P	TS1	Inter	TS2	P	TS1	Inter	TS2
B3LYP	6-311+G**	3.386	−31.720	−22.734	−22.684	0	−35.106	−26.120	−26.069
	Aug-CC-pVTZ	3.101	−31.494	−22.257	−29.969	0	−34.595	−25.358	−33.070
MP2	6-311+G**	10.719	−32.677	−28.586	−32.173	0	−43.397	−39.306	−42.892
	Aug-CC-pVTZ	6.078	−32.377	−28.762	−32.767	0	−38.4552	−34.84	−38.845
IS									
B3LYP	6-311+G**	−36.424	−32.642	−30.435	−54.367	0	3.781	18.750	−17.942
	Aug-CC-pVTZ	−36.992	−32.555	−30.357	−54.908	0	4.438	6.636	−17.916
MP2	6-311+G**	−30.144	−31.781	−36.269	−48.845	0	1.636	−6.125	−18.701
	Aug-CC-pVTZ	−35.517	−31.108	−37.109	−36.086	0	4.410	−1.592	−0.569

theory are employed. In addition to the Gaussian triple zeta basis set, the correlation consistent triple zeta, Aug-CC-PVTZ were also used. Results are compared to those obtained at the B3LYP/6-311+G** level of theory. This comparison is presented in Table 3 for both IO and IS. Figure 13 presents the variation of the relative energies of all critical points on the decomposition reaction path with the theoretical model used. It is evident from the data presented in Table 3 and Fig. 13 that the B3LYP/6-311++G** level of theory was able to capture the features of the decomposition reaction profile satisfactorily. The correspondence with the more expensive MP2 calculations is very good for the reactants, TS-1 and the products. This is true for both the IO and IS decomposition. However, the regions at which correlation energies dominate the interaction, i.e., the zwitterionic and TS-2 regions, the correspondence is not so good, yet the B3LYP/6-311++G**

Table 4 Summary of thermodynamic and kinetic properties of the decomposition reactions studied in the present work

Compound quantity	IO	IS	IIO	IIS
$\Delta H^{\#}$, kJ/mol	−13.898	145.696	−4.652	160.812
$\Delta G^{\#}_1$, kJ/mol	78.00	130.568	105.00	150.90
K_1, S^{-1}	13.289×10^{-2}	8.136×10^{-11}	2.463×10^{-6}	2.2057×10^{-14}
$t_{½}$, s	5.22	8.518×10^{9}	2.8×10^{5}	3.14×10^{13}
$\Delta G^{\#}_2$, kJ/mol	12.309	17.943	2.164	34.49
K_2, s^{-1}	4.33×10^{10}	1.964×10^{-9}	2.698×10^{11}	5.607×10^{6}
$t_{½}$, s	1.600×10^{-9}	3.528×10^{8}	2.569×10^{-10}	1.236×10^{-5}

Table 5 Calculated solvation and relative energies (kcal/mol^{-1}) of the reactant, intermediate, transition states for IIO and IIS decomposition reaction in solution using the B3LYP/6-311+G** level of theory. *DMSO* Dimethylsulfoxide, *DEE* diethylether

		Reactant	TS1	Inter	TS2
IIO					
Water	ΔE_{sol}	−11.625	−6.883	−8.932	−3.188
	ΔE_{re}	0.000	−27.271	−5.014	−2.755
DMSO	ΔE_{sol}	−11.412	−6.732	−8.889	−3.156
	ΔE_{re}	0.000	−27.208	−4.907	−2.742
DEE	ΔE_{sol}	−8.519	−4.994	−7.736	−2.392
	ΔE_{re}	0.000	−26.054	−4.322	−2.354
IIS					
Water	ΔE_{sol}	−11.226	−6.426	−8.184	−5.457
	ΔE_{re}	0.000	−39.445	−2.722	−12.761
DMSO	ΔE_{sol}	−10.937	−6.244	−7.980	−5.361
	ΔE_{re}	0.000	−39.337	−2.744	−12.653
DEE	ΔE_{sol}	−8.036	−4.649	−5.884	−4.067
	ΔE_{re}	0.000	−38.032	−3.245	11.850

level of theory still represents the reaction profile qualitatively. Using the augmented correlated triple basis set does not change the general picture much.

In conclusion, the theoretical model used in the present study is able to capture satisfactorily the features of the potential energy profile for the decompositions of IO and IS. Even at the region dominated by correlation interaction energies, the overall qualitative agreement is still satisfactory considering the much higher cost of other high level methods.

Table 7 Second-order delocalization energies $E^{(2)}$ for the studied compound (IIO) calculated at B3LYP/6-311+G** level of theory

	Donor	Acceptor	$E^{(2)}$/kcal/mol^{-1}
Reactant	LPO (2)	σ^*_{C1-C2}	24.74
	LPO (2)	σ^*_{C1-C3}	23.78
	LPO (1)	σ^*_{C1-C2}	4.43
	LPO (1)	σ^*_{C1-C3}	4.51
	σ_{C2-C3}	π^*_{C1-O}	89.49
	σ_{C1-C3}	σ^*_{C1-O}	3.23
	σ_{C1-C2}	π^*_{C5-C6}	27.21
	π_{C5-C6}	σ^*_{C2-C3}	19.36
TS1	LPO	σ^*_{C1-C3}	8.34
	σ_{C2-C3}	σ^*_{C1-O}	74.21
	σ_{C3-C1}	π^*_{C2-C5}	12.53
	σ_{C2-C3}	π^*_{C5-C6}	9.69
Inter	LPO	σ^*_{C1-C3}	6.6
	σ_{C2-C3}	σ^*_{C1-O}	48.54
	σ_{C1-C2}	σ^*_{C5-C6}	66.62
TS2	LPO	σ^*_{C1-C3}	3.77
	σ_{C2-C3}	σ^*_{C3-O5}	44.73
	π_{C1-O5}	σ^*_{C2-C3}	23.29

Conclusions

The electronic structure of IO has been investigated theoretically. The extraordinary stability of IO may very well be attributed to (1) the strong interaction between the C=C and the C=O bond orbitals and the consequent extension of the π-system; (2) the involvement of the C3 pz orbital in

Table 6 Some selected natural bond orbital (NBO) parameters computed at the B3LYP/6-311+G** level of theory for IO

Atom		Type(AO)	Occupancy	Energy	Atom natural electron configuration
C1	pz	Val(2p)	0.84385	−0.16312	[core]2S(1.03)2p(3.13)3d(0.01)
C2	pz	Val(2p)	0.84455	−0.16318	[core]2S(1.03)2p(3.13)3d(0.01)
C3	pz	Val(2p)	0.79963	−0.13446	[core]2S(0.76)2p(2.71)3S(0.01)3d(0.01)4p(0.02)
O6	pz	Val(2p)	1.49482	−0.24784	[core]2S(1.70)2p(4.87)3p(0.01)3d(0.01)
Donor			Acceptor	E^2	
BD C 1–C2			BD* C 3–O 6	28.13	
BD C 1–C2			BD* C 3–O 6	86.13	
BD C1–C3			BD* C 3–O 6	2.74	
LP (1)			RY*(1) C 3	16.93	
LP(2) O 6			BD*(1) C1–C3	24.04	
LP(2) O6			BD*(1) C2–C3	23.9	

Table 8 The second-order delocalization energies $E^{(2)}$ for the studied compound (IIS) calculated at B3LYP/6-311+G** level of theory

	Donor	Acceptor	$E^{(2)}$/kcal/mol^{-1}
Reactant	LPS	σ^*_{C1-C2}	11.54
	LPS	σ^*_{C1-C3}	11.76
	σ_{C1-C2}	σ^*_{C1-S}	104.30
	σ_{C2-C3}	σ^*_{C2-C5}	28.53
TS1	LPS	σ^*_{C1-C3}	19.67
	σ_{C1-C3}	σ^*_{C1-S}	99.79
	σ_{C5-C6}	σ^*_{C1-C2}	20.25
Inter	LPS	σ^*_{C1-C3}	63.85
	LPC2	σ^*_{C2-C3}	64.11
	σ_{C1-S}	σ^*_{C1-C3}	4.53
TS2	LPS	σ^*_{C1-C3}	5.29
	σ_{C1-C3}	π^*_{C1-S}	12.53
	σ_{C2-C3}	σ^*_{C6-C5}	192.24
	σ_{C1-S}	σ^*_{C2-C3}	23.29

tightening of binding and imparting an "aromatic character" to IO; in addition to (3) the contribution of the ionic resonance form IO-a to the resonance hybrid. This may also elaborate upon the suggestion of the "aromatic character" of IO.

The reaction mechanisms of the decomposition reaction of IO, its phenyl derivative (IIO) and its sulfur analogue (IIS) were investigated at the B3LYP/6-31++G** level of theory. All critical points on the reaction surface, reactants, transition states and intermediates were determined. NBO analysis was used to investigate the type and extent of interaction in studied species. The results indicate that the decomposition reaction occurs via a stepwise mechanism, with the formation of a short-lived intermediate. The character of the intermediate for the decomposition of IIO and IIS are different. In case of IIO decomposition, the intermediate structure is of prevailing zwitterionic character, whereas, that for the decomposition of IIS is of prevailing carbene character.

Acknowledgments This Project was funded by the Deanship of Scientific Research (DSR) King Abdulaziz University, Jeddah, under grant no. D19-130-/1432. The authors, therefore, acknowledge with thanks DSR support for Scientific Research.

References

1. Breslow R, Ryan G (1967) J Am Chem Soc 89:3073
2. Breslow R, Ryan G, Groves JT (1970) J Am Chem Soc 92:988
3. Breslow R, Oda M (1972) J Am Chem Soc 94:4787
4. Benson RC, Flygare WH, Oda M, Breslow R (1973) J Am Chem Soc 2772, and references therein
5. Oda M, Breslow R, Pecoraro J (1972) Tetrahedron Lett 4419
6. Breslow R, Oda M, Pecoraro J (1972) Tetrahedron Lett 4415
7. Yang J, McCann K, Laane J (2004) J Mol Struct 695–696:339–343
8. Brown FR, Finseth DH, Miller FA, Rhee KH (1975) J Am Chem Soc 97:1011
9. Tuazon EC, Finseth DH, Miller FA (1975) Spectrochim Acta 31A:1133
10. Benson RC, Flygare WH, Oda M, Breslow R (1973) J Am Chem Soc 95:2772
11. Komatsu K, Kitagawa T (2003) Chem Rev 103:1371
12. Poloukhtine A, Popik V (2003) J Org Chem 68:7833
13. Breslow R, Eischer T, Krebs A, Peterson RA, Posner J (1965) J Am Chem Soc 87:1320
14. Chiang Y, Kresge AJ, Popik V (1999) J Am Chem Soc 121:5930
15. Chiang Y, Kresge AJ, Paine SW, Popik V (1996) J Phys Org Chem 9:361
16. Wadsworth DH, Donatelliv BA (1981) Synthesis 285
17. Nguyen LT, DeProft F, Nguyen MT, Geerlings P (2001) J Chem Soc PerkinTrans 2:898
18. Poloukhtine A, Popik V (2006) J Phys Chem A110:1749
19. Eckart U, Sadlej AJ, Ingamells VE, Papadopoulos MG (2001) J Chem Phys 114
20. Breslow R, Altman LJ, Krebs A, Mohacsi E, Murata I, Peterson RA, Posner J (1965) J Am Chem Soc 87:1326
21. Dailey WP (1995) J Org Chem 60:6737
22. Andraos J, Chiang Y, Grant AS, Guo H-X, Kresge AJ (1994) J Am Chem Soc 116:7411
23. Chiang Y, Grant AS, Kresge AJ, Paine SW (1996) J Am Chem Soc 118:4366
24. Chiang Y, Grant AS, Guo H-X, Kresge AJ, Paine SW (1997) J Org Chem 62:5363
25. Chiang Y, Kresge AJ, Hochstrasser R, Wirz J (1989) J Am Chem Soc 111:2355
26. Chiang Y, Kresge AJ, Popik VV (1995) J Am Chem Soc 117:9165
27. Sung K, Fang D, Glenn D, Tidwell TT (1998) J Chem Soc Perkin Trans 2:2073
28. Frish MJ, Trucks GW, Schlegel HB, Scuseria GE, Robb MA, Cheeseman JR, Zakrzewski VG et al. (2008) Gaussian, Pittsburgh, PA
29. Zhang Q, Li Z, Chen B (2009) J Mol Struct (THEOCHEM) 901:202
30. Zhang Q, Chen B (2010) J Mol Struct (THEOCHEM) 941:10
31. Smith DM, Nicolaides A, Golding BT, Radom L (1998) J Am Chem Soc 120:10223
32. Hehre WJ, Radom L, Schleyer PVR, Pople JA (1986) Ab initio molecular orbital theory. Wiley, New York
33. Gonzalez C, Schlegel HB (1989) J Chem Phys 90:2154
34. Gonzalez C, Schlegel HB (1990) J Phys Chem 94:5523
35. Reed AE, Curtiss LA, Weinhold F (1988) Chem Rev 88:899–926
36. Lin L, Ding W-J, Fang W-H, Liu R-Z (2006) J Phys Chem A 110:8744–8749
37. Rochart WV, Gard GL (1969) J Org Chem 34:4173–4176
38. Ulic SE, Della Védova CO, Hermann A, Mack H-G, Oberhammer H (2008) J Phys Chem A 112:6211–6216
39. Reed AE, Weinhold F (1983) J Phys Chem 78:4066–4073
40. Chen XJ, Wu F, Yan M, Li HB, Tian SX, Shan X, Wang KD, Li ZJ, Xu KJ (2009) Chem Phys Lett 472(19):243–247
41. Frisch AE, Hratchian HP, Dennington RD II et al (2009) Gauss-View, Version 5.0.8. Gaussian, Wallingford
42. Elroby SAK, Osman OI, Aziz SG (2011) Mol Phys 109:1785–1795
43. Steinfeld JI, Francisco JS, Hase WL (1989) Chemical kinetics and dynamics, 2nd edn. Prentice Hall, Upper Saddle River, pp 300–301